https://doi.org/10.5194/egusphere-2025-4467
Preprint. Discussion started: 18 September 2025

A top-down evaluation of bottom-up estimates to reduce uncertainty in methane emissions from Arctic wetlands

Luana S. Basso[1], Goran Georgievski[2], Victor Brovkin[2], Christian Beer[3], Christian Rödenbeck[1], Mathias Göckede[1]

[1]Department of Biogeochemical Signals, Max Planck Institute for Biogeochemistry, Jena, 07745, Germany
[2]Department of Climate Dynamics, Max Planck Institute for Meteorology, Hamburg, 20146, Germany
[3]Department of Earth System Sciences, University of Hamburg, Hamburg, 20146, Germany

Correspondence to: Luana S. Basso (lbasso@bgc-jena.mpg.de)

Abstract.

Wetlands are a major natural source of atmospheric CH_4, however, accurately estimating their emissions is difficult due to the complex biogeochemical interactions and spatial heterogeneity of wetland environments. This study explores how a combination of atmospheric inverse and process-based modelling can reduce the discrepancy in Arctic wetland estimates between bottom-up and top-down approaches. We employed the Jena CarboScope global inversion system, incorporating prior wetland fluxes simulated by the JSBACH land surface model, which is part of the Max Planck Institute Earth System Model (MPI-ESM). We conducted a series of inversion experiments, each incorporating JSBACH-generated CH_4 fluxes based on different CH_4 production Q_{10} values to test the temperature sensitivity of emissions. Additionally, we examined the impact of changing the baseline f_{CH_4} fraction value, which defines the fraction of anaerobically mineralized carbon converted to CH_4, while keeping all other JSBACH and inversion settings constant. Our findings show that, at a pan-Arctic scale, using a CH_4 Q_{10} value of 1.8 produces the best agreement between the two approaches. However, no single Q_{10} value yielded optimal agreement between the simulated fluxes and the fluxes inferred from atmospheric observations across all subregions. Instead, the best performance varied spatially, with different CH_4 production Q_{10} values and baseline f_{CH_4} fraction leading to a better flux agreement in specific areas. These results highlight the importance of using regionally specific parameters to more accurately estimate wetland CH_4 emissions, and the potential of employing atmospheric inversions to guide bottom-up process models towards regionally representative parameter settings.

1. Introduction

Methane (CH_4) is the second most important anthropogenic greenhouse gas and it is emitted from both natural and anthropogenic sources. Combined wetlands and inland freshwaters are the largest natural source of CH_4 to the atmosphere, accounting for about 28-37% (by bottom-up and top-down estimates, respectively) of the global total CH_4 emissions (Saunois et al., 2025). However, quantifying these emissions remains challenging due to the complexity of biogeochemical processes and the spatial variability of these ecosystems. Process-model ensemble estimates indicate that, between 2010 and 2020, wetlands emitted approximately 158 ± 24 $TgCH_4\ y^{-1}$. This represents an increase of ~5 $TgCH_4\ y^{-1}$ compared to the 2000-2009 average, with the most substantial increases observed in tropical regions, followed by mid- and high-latitude areas (Zhang et al., 2025).

Global and regional CH_4 emissions are estimated using both bottom-up or top-down approaches. Bottom-up methods, including data-driven ecosystem flux upscaling and process-based models, provide detailed information with fine-scale resolution for both, processes and spatial heterogeneity. Process-based models simulate CH_4 emissions by mathematically representing ecosystem dynamics, biogeochemical cycles, and physical processes. Nevertheless, it is challenging to extrapolate these estimates to regional or global scales because wetland characteristics (e.g., extent, hydrology and vegetation) vary substantially across space, and simulated CH_4 fluxes are highly sensitive to the choice of model parameterizations. Mechanistic modeling of net surface CH_4 emissions requires capturing a range of complex, interacting processes (Conrad, 1999; Moser et al., 2025; Riley et al., 2011).

Anaerobic CH_4 production is the result of a number of biogeochemical processes that take place in a chain or in parallel (Conrad, 2020; Moser et al., 2025; Song et al., 2020). After an enzymatic breakdown of macromolecules, fermentation of the resulting dissolved organic matter (DOC) leads to acetate, hydrogen and CO_2. In either acetoclastic or hydrogenotrophic methanogenesis, these byproducts are immediately further used to finally produce CH_4 and CO_2 (Conrad, 2020). In addition, alternative electron acceptors, such as Fe-III can be utilized by microbes to produce CO_2 from acetate (Sulman et al., 2022; Zheng et al., 2019). The net CH_4:CO_2 production ratio is therefore determined by the relative importance of these underlying processes, which in turn are dependent on environmental conditions. That is why in laboratory incubation experiments, a large range of this production ratio has been observed (Knoblauch et al., 2018). After production, CH_4 may be consumed by methanotrophic bacteria (Knoblauch et al., 2015; Riley et al., 2011) or transported to the atmosphere via plant aerenchyma, ebullition, or diffusion through soil or water (Kaiser et al., 2017; Walter and Heimann, 2000; Wania et al., 2010). That leads to a CH_4:CO_2 emission ratio at the surface which is different from the CH_4:CO_2 production ratio. Since underlying biogeochemical processes are very complex and dependent on detailed environmental conditions, global-scale land surface models usually represent anaerobic CH_4 production as a first-order decay of soil organic matter with adjusted rate constants. And then, a fixed ratio of CH_4 versus CO_2 production out of that decomposition is applied (Guimberteau et al., 2018; Kleinen et al., 2020; Moser et al., 2025; Ricciuto et al., 2021; Sellar et al., 2019). Here, the models can differ in whether the ratio applies to the CH_4 production or emission. The JSBACH v3.2 (Reick et al., 2021) that we apply in this study is taking the first approach and mechanistically distinguish between methanogenesis and methanotrophy.

Developing these models requires balancing the inclusion of key mechanisms with limitations such as structural and parameter uncertainty, spatial heterogeneity, sparse observational data, uncertain initial and boundary conditions, and computational constraints (Riley et al., 2011). Previous studies have shown that CH_4 emissions are highly sensitive to parameters regulating microbial production and oxidation processes (Chinta et al., 2024; Riley et al., 2011; Song et al., 2020). A higher CH_4:CO_2 ratio indicates a greater dominance of CH_4 in production and emission relative to CO_2 (Chinta et al., 2024). Based on anaerobic incubations of thermokarst lake sediments, Gonzalez Moguel et al. (2025) observed that the $\Delta^{14}C$ values

https://doi.org/10.5194/egusphere-2025-4467
Preprint. Discussion started: 18 September 2025

of both CH_4 and CO_2 showed strong positive correlations with net CH_4 production rates and CH_4:CO_2 ratios. This indicates that CH_4 production occurs faster and at a higher rate when younger organic matter decomposes. These patterns suggest that the presence of younger carbon substrates increases methanogenesis compared to overall fermentation and anaerobic respiration (Gonzalez Moguel et al., 2025). A higher CH_4 production Q_{10} indicates that CH_4 production increases more rapidly with rising temperatures. This can indirectly enhance diffusive fluxes by creating larger concentration gradients between the soil and the atmosphere (Chinta et al., 2024). However, as regional model sensitivity varies and site-specific measurements may not be representative across broader areas, CH_4 production Q_{10} are uncertain at large spatial scales. For example, increasing CH_4 production Q_{10} in high-latitude regions can reduce simulated CH_4 emissions by more than half, because the temperature-dependent component, scaled relative to a reference temperature of 295 K, leads to a decline in CH_4 production rate at the lower temperatures typical of these regions (Riley et al., 2011). In contrast, the opposite pattern is observed in tropical regions (Riley et al., 2011). Many large-scale land surface models still rely on simplified, fixed CH_4 production fractions, which limits their ability to accurately represent observed spatiotemporal variability in CH_4:CO_2 production ratios across Arctic landscapes (Moser et al., 2025). These differences in model structure, parameterization and initialization contribute strongly to relative high uncertainties in wetland estimates (Poulter et al., 2017).

In JSBACH v3.2, anaerobic decomposition and CH_4 oxidation are temperature dependent. However, in addition to that, the CH_4:CO_2 production ratio is also assumed to follow a Q_{10} temperature sensitivity (Kleinen et al., 2020). That means that we assume that the relative importance of the above-mentioned underlying biogeochemical processes changes in space and time depending on the soil temperature. In addition, making the CH_4:CO_2 production ratio temperature dependent allows us to additionally tune CH_4 versus CO_2 production across bioclimatic zones. One big research question now is, how high should be the Q_{10} value for this temperature dependency of the CH_4:CO_2 production ratio? In order to answer such question, we employ a novel integration of bottom-up and top-down approaches.

Top-down approaches estimate net surface-atmosphere CH_4 fluxes using atmospheric observations (in situ, flask and/or satellite measurements) in combination with prior flux information (from process-based models and/or inventories), and atmospheric transport and chemistry models to link surface sources with atmospheric observations. Their ability to provide accurate estimates of net surface-atmosphere fluxes is limited by sparse observational coverage, particularly in remote regions, as well as by uncertainties in atmospheric transport, prior flux estimates, and atmospheric CH_4 sink processes (Houweling et al., 2017). These limitations can lead to significant uncertainties in the magnitude and spatial distribution of inferred emissions, which makes attributing fluxes to specific sources or processes challenging. Still, despite these limitations, the inverse modeling approach allowed us to derive important constraints on the global sources and sinks of CH_4 (Houweling et al., 2017).

Substantial discrepancies exist between bottom-up and top-down estimates of CH_4 emissions. From 2010 to 2019, top-down approaches estimated global CH_4 emissions at 575 $TgCH_4\ y^{-1}$ (553-586 $TgCH_4\ y^{-1}$), whereas bottom-up estimates were approximately 15% higher, at 669 $TgCH_4\ y^{-1}$ (512-849 $TgCH_4\ y^{-1}$) (Saunois et al., 2025). These differences, despite the fact that bottom-up results are used as prior in top-down approaches, point to additional constraints of bottom-up CH_4 flux estimates by atmospheric observations. For example, important large-scale CH_4 uptake by upland soils (Juncher Jørgensen et al., 2024;

Voigt et al., 2023) is usually underrepresented in land surface models (D'Imperio et al., 2023; Song et al., 2024). More generally, we assume that bottom-up approaches are still very limited in their ability to upscale the complex and spatially varying processes underlying CH_4 emissions. In boreal regions, inland freshwater sources dominate CH_4 emissions, accounting for 41% and 54% in top-down and bottom-up budgets, respectively (Saunois et al., 2025). Similarly, Hugelius et al. (2024) reported substantial discrepancies between bottom-up and top-down CH_4 emission estimates for the Arctic–boreal region, with 50 $TgCH_4\ y^{-1}$ (29-71 $TgCH_4\ y^{-1}$) for bottom-up and 20 $TgCH_4\ y^{-1}$ (15-24 $TgCH_4\ y^{-1}$) for top-down. Despite recent efforts to improve monitoring networks and modeling frameworks, significant discrepancies remain between these approaches. Still, top-down approaches can be used to assess the representativeness of bottom-up fluxes and their underlying parameterizations on a large scale. Combining information from both methods can therefore help to reconcile discrepancies and improve the consistency of CH_4 emission estimates at different spatial scales.

This study explores the use of atmospheric inverse modeling to constrain bottom-up estimates of wetland CH_4 emissions in the Arctic-Boreal region. Using the Jena CarboScope global inversion system, we employed prior fluxes from the JSBACH land surface model (a component of the MPI Earth System Model) and systematically varied key parameters that govern CH_4 production. Specifically, we tested a range of Q_{10} values, which define the temperature sensitivity of CH_4 production, and different f_{CH_4} baseline values, which determine the proportion of anaerobically mineralized carbon converted to CH_4. We kept other model settings constant throughout these tests. Integrating these parameter sensitivity experiments into the inversion framework allowed us to assess which parameterizations yield the most consistent fluxes with atmospheric observations. This approach enables us to identify regionally representative parameter settings and guide parameterizations that could improve the consistency between bottom-up process models and top-down constraints on Arctic-Boreal wetland CH_4 emissions.

2. Methods

2.1. Region and time period of interest

Our Arctic-Boreal domain was defined based on The Boreal-Arctic Wetland and Lake Dataset – BAWLD (Olefeldt et al., 2021), and we divided this region into 6 sub-regions for more detailed spatial analyses (Alaska, western Canada, eastern Canada, Europe, western Russia, eastern Russia, Fig. 1). In recent decades, the atmospheric observation network suitable for inverse modeling has expanded across the Arctic, with a considerable increase in available sites after 2010 (Vogt et al., 2025). However, due to data-sharing disruptions associated with the ongoing conflict involving Russia and Ukraine, observational data from Russian stations has been limited since 2022. Consequently, this study focuses on the period from 2010 to 2021, when data coverage was more consistent across the full domain.

https://doi.org/10.5194/egusphere-2025-4467
Preprint. Discussion started: 18 September 2025

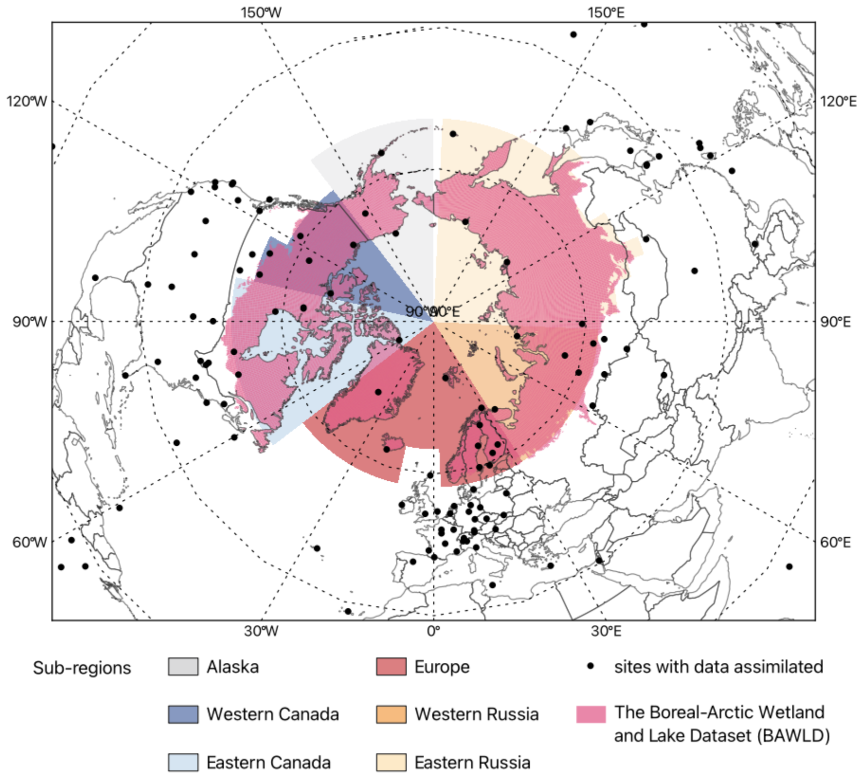

Figure 1: Geographic distribution of surface sites operated by different network providers where flask-based and/or continuous in-situ CH_4 measurements are available for assimilation into the inverse model (black dots). The colored boxes delineate the Arctic-Boreal regions (Alaska, western Canada, eastern Canada, Europe, western Russia, eastern Russia), as defined based on The Boreal–Arctic Wetland and Lake Dataset (BAWLD) (Olefeldt et al., 2021).

2.2. Wetland estimates used as prior fluxes in the inverse modelling

In this study, we utilize the JSBACH model (Reick et al., 2021), the land component of the MPI-ESM (Mauritsen et al., 2019), to estimate bottom-up wetland CH_4 emissions. Originally, JSBACH was developed as a lower boundary condition for the atmospheric component of the MPI-ESM; however, it has since been updated to function as a standalone land surface model driven by observed climate data to simulate terrestrial components of the carbon, energy and water cycles. In this study, simulations conducted at T63 resolution (approximately 1.85°, or 185 km) were driven using the CRUJRA2.3 (Harris, 2019) climate data. A multilayer vertical soil profile is implemented as described by Hagemann and Stacke (2015), while features relevant for high-northern latitudes permafrost have been implemented by Ekici et al. (2014). The Richards' equation (Richards, 1931), along with thermal diffusion, governs the vertical distribution of moisture and heat in the soil (Reick et al., 2021). Soil organic carbon (SOC) decomposition is simulated as a first-order decay process that depends on surface air

https://doi.org/10.5194/egusphere-2025-4467
Preprint. Discussion started: 18 September 2025

temperature, water availability, and litter size, following the YASSO model formulation (Tuomi et al., 2011) and its implementation in JSBACH by Goll et al. (2015).

The wetland area fraction of the grid is determined using TOPMODEL (Beven and Kirkby, 1979), a conceptual rainfall-runoff model that estimates inundation based on the compound topographic index (CTI). If the inundated fraction of the grid is non-frozen (depending on the soil temperature), it is considered a CH_4-emitting area. The methodology for wetland CH_4 production and transport is adopted from Riley et al. (2011), and the details of the TOPMODEL and its implementation for wetland CH_4 within JSBACH are outlined in Kleinen et al. (2020). TOPMODEL assumes a constant exponential decline of transmissivity with depth, defined as the ratio of the difference between the local sub-grid-scale CTI and the mean grid-cell CTI to the difference between their corresponding local sub-grid-scale water table and mean grid-cell water table (see equation (1) in Kleinen et al. (2020)). As water propagates from the surface, it saturates the soil layers based on volumetric moisture content and field capacity. Starting from the bottom of the soil column, the mean grid-cell water table is located in the first soil layer where the layer saturation is below the experimentally determined saturation threshold. The sensitivity study indicates that using CRUJRA (Harris, 2019) as the forcing data, setting the saturation threshold at 7.25, configuring the exponential decline of transmissivity with depth to 4, and limiting the valid range of CTI to values greater than 5.5 results in a reasonable estimation of present-day wetland extents.

In JSBACH, carbon enters the soil as litter, both above- and belowground, originating from decomposing vegetation. This carbon eventually returns to the atmosphere through decomposition processes as CO_2 and CH_4 emissions. Carbon fixed by vegetation is allocated to green tissue (leaves, fine roots), wood (stems, branches), and reserve pools (e.g., sugars and starches). Routine turnover, herbivory, and root exudation transfer carbon into above- and belowground litter pools. Depending on the plant functional type (PFT), litter carbon is distributed among acid-soluble, water-soluble, ethanol-soluble, and non-soluble pools, each further divided into above- and belowground fractions, as well as a humus pool. Decomposition rates vary based on temperature, precipitation, and litter size. Under anoxic conditions (in the inundated fraction of the tile), SOC decomposes into both CO_2 and CH_4. The baseline rate of SOC decomposition under anaerobic conditions is reduced compared to aerobic conditions. Temperature dependency of CH_4 production as part of SOC decomposition follows the Q_{10} model with a reference temperature of 295K (Equation 1). The fraction of CH_4 production is capped at 0.5; that is, no more than 50% of carbon can be converted to CH_4. However, the CH_4:CO_2 ratio of net emissions to the atmosphere is typically lower than the ratio of gross production due to oxidation (methanotrophy) and differences in transport pathways. Oxidation, which follows Michaelis-Menten kinetics (with $Q_{10} = 1.9$, which remained constant throughout the sensitivity tests), converts a portion of CH_4 to CO_2, thus increasing CO_2 and decreasing CH_4 emissions. Transport mechanisms further differentiate the fate of these gases: CH_4 can escape via diffusion, plant-mediated transport, or ebullition, whereas CO_2 is not released through ebullition. O_2 availability and soil moisture regulate the efficiency of CH_4 oxidation. Therefore, the net CH_4:CO_2 emission ratio depends on the combined effects of CH_4 production, oxidation, and transport processes. Warmer, oxic conditions tend to reduce the net CH_4:CO_2 (due to stronger aerobic oxidation of CH_4), while colder or persistently anoxic, saturated conditions (with ebullition) can increase

https://doi.org/10.5194/egusphere-2025-4467
Preprint. Discussion started: 18 September 2025

the net CH_4:CO_2 ratio compared to cases with strong oxidation. Equation 1 shows how the Q_{10} law controls the CH_4 fraction (f_{CH_4}) as a function of soil temperature (T_{soil}) and the baseline fraction (baseline f_{CH_4} fraction):

$$f_{CH_4} = f_{CH_4,baseline} \cdot Q_{10}^{(T_{soil}-295)/10K} \qquad \text{Equation 1}$$

To evaluate how sensitive CH_4 wetland emission estimates are to key parameters, we conducted nine experiments in which we varied only the Q_{10} coefficient for CH_4 production and the baseline f_{CH_4} fraction (Fig. 2b). Specifically, we tested three different Q_{10} values ranging from 1.4 to 2.2 and baseline f_{CH_4} fractions from 0.33 to 0.38. These combinations are summarized in Table 1 and were chosen to identify parameter sets that best align with the observed atmospheric data.

2.3. Inverse modeling setup

We used the Jena CarboScope Inversion System (Rödenbeck, 2005) to quantify CH_4 emissions between the surface and the atmosphere globally from 2010 to 2021, with the evaluation and interpretation of fluxes focused on the Arctic-Boreal region. This is a linear Bayesian framework that infers surface–atmosphere CH_4 fluxes based on observed atmospheric mole fractions. A total of 154 stations were assimilated for the global domain (Fig.1). These CH_4 observations were obtained from several global and regional networks (ICOS RI et al., 2024; Schuldt et al., 2023), with the majority of sites located in the Northern Hemisphere, including 33 stations within the Arctic–Boreal domain. For tower sites with multiple intake heights available, we assimilated only data from the highest height in the inversion, and for the continuous data, we use only daytime measurements. The transport model used in CarboScope is the TM3 global atmospheric tracer model (Heimann and Körner, 2003) and is driven by meteorological inputs from the NCEP reanalysis dataset (Kalnay et al., 1996). Flux inversions were conducted at a spatial resolution of approximately 3.8° latitude by 5° longitude, with 19 vertical layers and a daily temporal resolution. To account for model-data mismatch, including the representation error of the measurements within the transport model, we assigned an uncertainty of 30 ppb. Additionally, to ensure balanced representation across observational sites, particularly between continuous and sparse time series, we applied a data density weighting scheme, assigning equal influence to each weekly period, regardless of data frequency (Rödenbeck, 2005).

Prior CH_4 flux estimates include five source categories, all of which were optimized: wetlands, other natural sources, anthropogenic, ocean and fire emissions. The monthly mean emissions from wetlands and fires were obtained from the JSBACH model (Kleinen et al., 2020), as previously described. Additional natural sources, such as termites and wild animal emissions taken from JSBACH (Kleinen et al., 2020) and geological emissions from Etiope et al. (2019) were combined as the "other natural source" category. Emissions from oceans were obtained from Weber et al. (2019) and implemented as a non-seasonal climatology. Anthropogenic emissions were obtained from the EDGAR inventories database (https://edgar.jrc.ec.europa.eu) version 8 (IEA et al., 2024) and are provided as monthly global fluxes. This category includes emissions from agriculture, livestock, waste management, fossil fuel exploitation and other minor anthropogenic sources except biomass burning.

CH_4 chemical loss includes loss due to OH and Cl in the troposphere, as well as OH, Cl, and $O(^1D)$ in the stratosphere. For tropospheric OH, we use the monthly three-dimensional OH fields calculated by Spivakovsky et al. (2000), which are based on observed climatological distributions of OH precursors and scaled to match the observed CH_3CCl_3 lifetime. The monthly climatological loss rates of CH_4 in the stratosphere due to OH, Cl, and $O(^1D)$ were derived from a simulation of the ECHAM5/MESSy1 chemistry transport model (Jöckel et al., 2006). Additionally, tropospheric Cl loss is simulated using a recent model-derived estimate of tropospheric Cl (Hossaini et al., 2016). The surface sink from upland soils and the ocean was implemented as a zeroth-order reaction with prescribed reaction rates that occur only in the surface-most model layer. Reaction rates for the microbial oxidation of atmospheric CH_4 in soil were based on the uptake estimates from the LPJ-Bern model (Spahni et al., 2011).

2.4. Evaluating Bottom-Up Emissions Using Top-Down Constraints

Previous studies have used atmospheric inversion models to evaluate in between different bottom-up estimates which one best reproduce observed atmospheric CH_4 data (e.g., Kim et al., 2011; Miller et al., 2016), providing an effective framework for model evaluation. In this study, we evaluated the performance of different JSBACH parameterizations by using the CH_4 wetland emission outputs from each experiment as wetland prior fluxes in a top-down atmospheric inversion framework. The inversion then generated posterior fluxes, reflecting the adjustments needed to align the prior emissions with atmospheric CH_4 observations. In this study, we used the model adjustment defined as the difference between posterior and prior fluxes, calculated as the mean monthly and mean annual values across the Arctic–Boreal region from 2010 to 2021. First, we identified the parameterization resulting in the lowest mean model adjustment across the entire domain. For the monthly analysis, we first computed the mean monthly prior flux and the mean monthly posterior flux, and then defined the model adjustment as the difference between these two means. For the annual analysis, we calculated the mean annual prior and posterior fluxes and again defined the adjustment as their difference. This allowed us to determine which JSBACH configuration provided the best overall agreement with atmospheric constraints at the pan-regional scale and investigate temporal variability. Next, we examined spatial variability of the difference between posterior and prior fluxes using different JSBACH parameterizations as wetland priors. At the grid-cell level, we identified the parameter combination that minimized annual model adjustment, thereby providing the best match to the top-down atmospheric constraints. To conduct this analysis, an ensemble of posterior fluxes was calculated based on each CH_4 production Q_{10} value from the prior wetland flux. This approach was supported by the observation that CH_4 production Q_{10} significantly influenced CH_4 emission estimates compared to the baseline f_{CH_4} fraction. Additionally, posterior fluxes from priors with different baseline f_{CH_4} fraction scenarios remained highly similar for a given Q_{10} value. As a result, maps were made by calculating the absolute difference between the posterior ensemble of

https://doi.org/10.5194/egusphere-2025-4467
Preprint. Discussion started: 18 September 2025

the respectively Q_{10} value and prior CH_4 fluxes for each experiment at each grid-cell. Then, the annual mean adjustment was calculated and we identified the parameterization that resulted in the smallest adjustment at each grid-cell. In summary, each grid-cell shows the experiment that best matched the atmospheric CH_4 observations.

3. Results and Discussion

3.1 Sensitivity of JSBACH CH_4 wetland emission estimates to CH_4 production Q_{10} and baseline f_{CH_4} fraction in Arctic–Boreal region

Table 1 summarizes the experiments and parameters combinations that have been tested in the JSBACH model and used as a wetland prior in the atmospheric inversions. Across the Arctic-Boreal region, our nine experiments produced annual mean CH_4 wetland estimates ranging from 13.8 to 33.5 $TgCH_4\ y^{-1}$. These estimates are consistent with previously published bottom-up estimates of ~15-50 $TgCH_4\ y^{-1}$ per year, with most studies reporting mean values near 20-25 $TgCH_4\ y^{-1}$ (Christensen et al., 1996; Ying et al., 2025; Yuan et al., 2024; Zhang et al., 2025). It should be noted that these studies consider different spatial domains and time periods. The estimates obtained using a Q_{10} value of 1.8 align most closely with this published range among our experiments.

Table 1. Summary of JSBACH wetland CH_4 estimates used as prior fluxes in the inversions and posterior fluxes estimates for each respective model run.

Experiment	JSBACH parameterization		Arctic-Boreal annual mean CH_4 emission ($TgCH_4\ y^{-1}$)*		
	Baseline f_{CH_4} fraction	Q_{10} model	JSBACH estimates (prior)	Posterior estimates	Mean model adjustment
B1_low	0.33	1.4	31.7 ± 1.1	25.0 ± 1.4	-6.7
B1_mid	0.33	1.8	20.0 ± 0.7	22.9 ± 1.1	2.9
B1_high	0.33	2.2	14.6 ± 0.5	21.2 ± 0.9	6.6
B2_low	0.35	1.4	29.7 ± 0.9	24.8 ± 1.5	-5.0
B2_mid	0.35	1.8	18.9 ± 0.6	22.7 ± 1.1	3.8
B2_high	0.35	2.2	13.8 ± 0.5	20.9 ± 0.9	7.1
B3_low	0.38	1.4	33.5 ± 1.0	25.2 ± 1.6	-8.2
B3_mid	0.38	1.8	21.3 ± 0.7	23.3 ± 1.2	2.0
B3_high	0.38	2.2	15.5 ± 0.5	21.6 ± 1.0	6.1

*The annual mean between 2010 and 2021, with the standard deviation representing interannual variability.

Emissions peaked during the summer months (July-August), with a mean emission ranging from 6.8 to 14.1 $TgCH_4$ y^{-1} (Fig. 2b). These larger emissions were followed by spring (May-June; range of 3.5-7.8 $TgCH_4$ y^{-1}), autumn (September-October; range of 2.8-7.7 $TgCH_4$ y^{-1}), and winter with the lower emissions (November-April; range of 0.4-1.5 $TgCH_4$ y^{-1}). The timing of the peak in wetland emissions aligns with previous bottom-up estimates (Ying et al., 2025). At the sub-regional scale, emissions showed substantial spatial variability (Fig. 2c). The highest annual mean fluxes were found in western Russia (3.4-8.7 $TgCH_4$ y^{-1}, depending on the parameter set), followed by eastern Canada (3.4-8.2 $TgCH_4$ y^{-1}), eastern Russia (3.1-7.2 $TgCH_4$ y^{-1}), western Canada (1.8-4.4 $TgCH_4$ y^{-1}), Europe (1.5-3.4 $TgCH_4$ y^{-1}), and Alaska (0.5-1.6 $TgCH_4$ y^{-1}).

In general, increasing the baseline value of the f_{CH_4} fraction from 0.33 to 0.38 increases CH_4 production. However, an increase in the CH_4 production Q_{10} parameter decreases CH_4 production for temperatures below 295 K (the reference temperature) and increases it for temperatures higher than 295 K. This means that increasing Q_{10} values from 1.4 to 2.2 reduces wetland CH_4 emissions in the comparatively cold Arctic region (Table 1 and Fig. 2). The sensitivity of wetland CH_4 to the Q_{10} temperature response and the baseline f_{CH_4} fraction is evident when comparing seasonal cycles over the Arctic-Boreal domain (Fig. 2b). For example, contrasting the simulations with baseline f_{CH_4} fraction equaling 0.33 and varying CH_4 production Q_{10} values (from 1.4 to 2.2), shows that increasing Q_{10} significantly reduces annual wetland mean CH_4 emission in this region by ~ 54% (~17 $TgCH_4$ y^{-1}). This reduction is not uniform throughout the year. Although winter emissions are relatively low, increasing Q_{10} from 1.4 to 2.2 results in a ~72% decrease compared to a ~50-59% decrease during the summer, spring and fall. Similarly, the influence of the baseline f_{CH_4} fraction can be observed by keeping Q_{10} constant, for example at 1.4, and varying the baseline f_{CH_4} fraction from 0.33 to 0.38. This increase leads to an increase of up to 6% in the annual wetland CH_4 emissions for the region. In general, our parameter sensitivity tests show that CH_4 production Q_{10} has a stronger effect on emission variability than the baseline f_{CH_4} fraction. These wetland CH_4 emission estimates with different parameterizations were subsequently integrated into the Jena CarboScope atmospheric inversion framework as wetland prior fluxes to determine the combination that closest align with atmospheric CH_4 observations, which means those requiring the minimum adjustment to fluxes from prior to posterior.

https://doi.org/10.5194/egusphere-2025-4467
Preprint. Discussion started: 18 September 2025

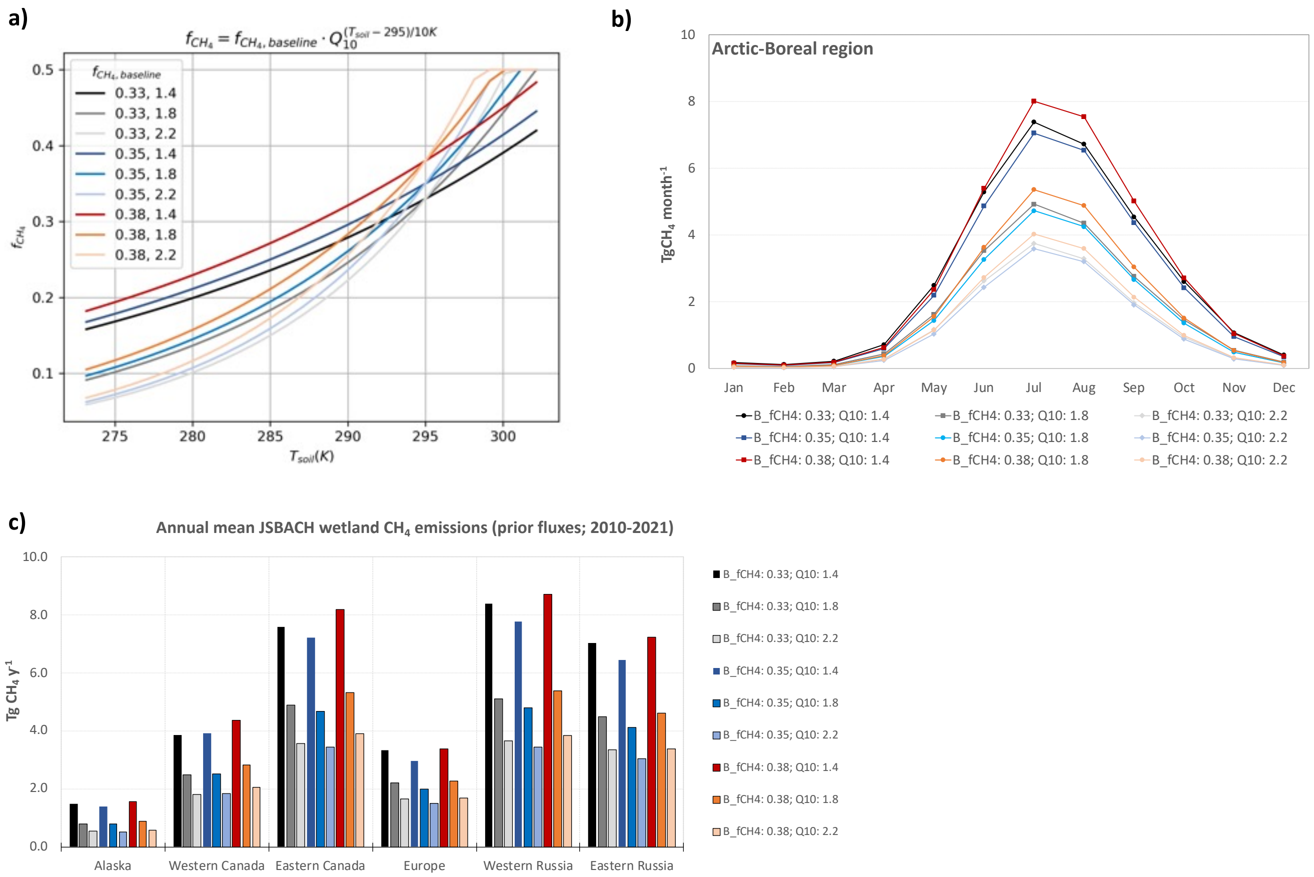

Figure 2. a) Sensitivity of f_{CH_4} production fraction to the chosen range of input parameters for this study. The y-axis represents the fraction of anaerobic carbon mineralization allocated to CH_4 production, calculated using the equation displayed at the top of the panel and in Equation 1. In the legend, the first number denotes the f_{CH_4} baseline fraction and the second number denotes the CH_4 production Q_{10} value. b) Mean seasonal cycle of Arctic-Boreal wetland CH_4 emissions for each experiment used in the inversion as the wetland prior flux. c) Annual mean wetland fluxes from each experiment estimated by JSBACH model.

3.2 Evaluation of JSBACH CH_4 Fluxes Using Inverse Modeling

Our nine inverse model estimates produce an annual mean total emission (i.e. including natural and anthropogenic sources) for the Arctic-Boreal region ranging from 44.2 to 47.1 $TgCH_4\ y^{-1}$, with wetland emissions being the main CH_4 source to the atmosphere. Depending on the parameter set in prior flux setup by JSBACH, the annual mean wetland emission ranges from 20.9 to 25.0 $TgCH_4\ y^{-1}$ (47-54% of total emissions). The largest posterior wetland CH_4 emissions were estimated for western Russia (range of 6.9-8.4 $TgCH_4\ y^{-1}$, depending on the parameter set), followed by eastern Russia (range of 6.0-7.5 $TgCH_4\ y^{-1}$), eastern Canada (range of 4.3-4.9 $TgCH_4\ y^{-1}$), western Canada (range of 1.7-1.8 $TgCH_4\ y^{-1}$), Alaska (range of 1.0-2.0 $TgCH_4\ y^{-1}$) and Europe (range of 0.7-0.8 $TgCH_4\ y^{-1}$)

At the pan-Arctic scale, posterior wetland fluxes are higher than prior fluxes in the experiments using CH_4 production Q_{10} values of 1.8 (8-22% higher than prior) and 2.2 (37-54% higher), see Table 1 and Fig. 3a. This suggests that these prior

https://doi.org/10.5194/egusphere-2025-4467
Preprint. Discussion started: 18 September 2025

estimates underestimate CH_4 emissions in the Arctic–Boreal region relative to the observation-constrained posterior fluxes. However, prior fluxes estimated using a Q_{10} value of 1.4 are higher than posterior fluxes (16-25% higher than posterior), indicating overestimation of CH_4 emissions in this case. When comparing the model adjustment for the three experiments (varying only the Q_{10} parameters), the prior flux using Q_{10} values of 1.8 produces the best agreement between prior and posterior flux budgets, meaning that a minimum adjustment in the inverse model optimization is required when considering annual mean emissions in the entire Arctic-Boreal region. Additionally, when comparing the different baseline f_{CH_4} fractions (using the Q_{10} value with the best fit: 1.8), the minimum adjustment in the inverse model optimization is required for the prior flux with the largest baseline f_{CH_4} fraction (0.38), with posterior flux being 8% (2.0 $TgCH_4\ y^{-1}$) higher than the prior.

Our posterior estimates of CH_4 emissions from wetlands are similar to previous Arctic-Boreal estimates. Using a process-oriented ecosystem model, Christensen et al. (1996) estimated a total CH_4 emissions from northern wetlands and tundra (> 50°N) to be 20 ± 13 $TgCH_4\ y^{-1}$. Yuan et al. (2024) reported a mean annual emission of 20.3 ± 0.9 $TgCH_4\ y^{-1}$ from boreal-Arctic wetland based on upscaled flux observations for the period 2002-2021. The Global Carbon Project estimated a mean annual wetland (including inland freshwaters) CH_4 emission for regions north of 60°N at 24 (9-53) $TgCH_4\ y^{-1}$, while top-down approaches resulted in a lower estimate of 9 (7-17) $TgCH_4\ y^{-1}$ for the same region (Saunois et al., 2025). Recently, Ying et al. (2025) estimated an annual mean CH_4 emissions from vegetated wetlands north of 45°N during 2016-2022 at 22.8 ± 2.4 $TgCH_4\ y^{-1}$, ranging from 15.7 ± 1.8 $TgCH_4\ y^{-1}$ to 51.6 ± 2.2 $TgCH_4\ y^{-1}$, depending on the wetland dataset used in the machine-learning-based upscaling approach. Although our posterior estimates are within the range of previous Arctic-Boreal estimates, direct comparisons are difficult because of differences in the study period, methodological approach, and inconsistent or unclear definitions of the spatial domain.

3.3 Seasonal variability in optimum CH_4 production Q_{10} settings

Before analyzing regional differences in optimum CH_4 production Q_{10} settings, we first focused on a clear seasonal pattern in the adjustments between prior and posterior CH_4 emissions, which showed a peak of changes occurring during summer. We therefore assessed whether the Q_{10} value resulting in the minimum adjustment remained constant throughout the year or varied by season. At a pan-Arctic scale, seasonal variations were evident: estimates using CH_4 production Q_{10} equaling 1.8 aligned better with atmospheric observations in spring and fall but substantially underestimated summer emissions (Fig. 3b). In contrast, estimates using a Q_{10} of 1.4 best agreed well with the atmospheric observation during summer, reducing the discrepancy between top-down and bottom-up estimates during the growing season, but strongly overestimating emissions in spring and fall (Fig. 3b). This pattern is primarily driven by wetlands in Russia. Bergman et al. (2000) found temporal variation in Q_{10} at peatland sites, suggesting that factors such as the availability of easily degradable compounds (e.g., root exudates) and the activity of anaerobic microbial biomass influence CH_4 production rates alongside temperature.

https://doi.org/10.5194/egusphere-2025-4467
Preprint. Discussion started: 18 September 2025

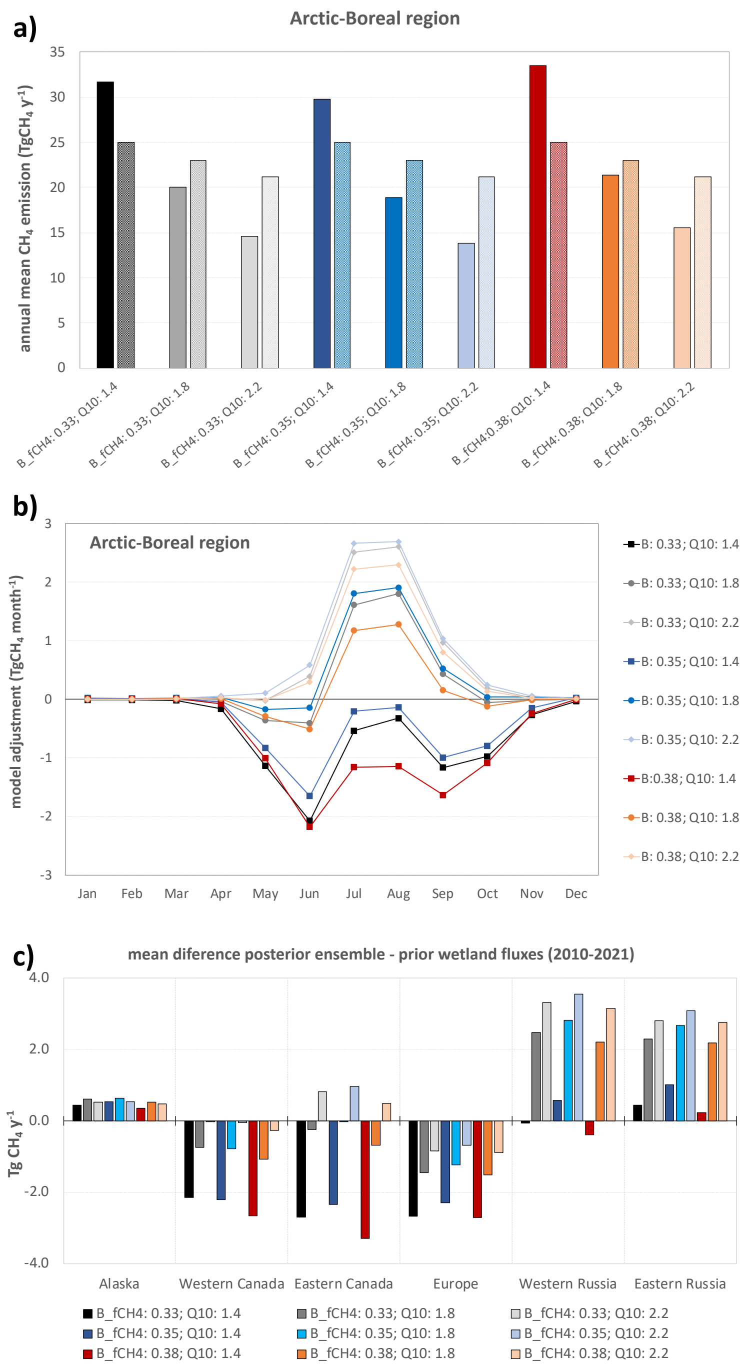

Figure 3. a) Annual mean CH_4 emissions (prior: full color bars; posterior: light color bars) for the entire Arctic-Boreal region using different values of Q_{10} parameter and baseline f_{CH_4} fraction in JSBACH wetland emissions. b) adjustment of prior fluxes at monthly timesteps for the same model configurations as used in (a). c) annual mean model adjustment (posterior minus prior flux) for each one of the sub-regions. Positive values indicate regions where prior estimates underestimated emissions compared with posterior estimates, while negative values represent areas where prior emissions overestimate CH_4 emissions compared with the posterior estimates.

https://doi.org/10.5194/egusphere-2025-4467
Preprint. Discussion started: 18 September 2025

3.4. Spatial patterns of best-fit model results based on posterior fluxes

CH_4 emissions exhibited spatial variability, and model adjustments were not uniform across the domain. This suggests that the optimal parameterization varies by region and seasons (as discussed in Section 3.3). In some areas, Q_{10} values of 1.4 or 2.2 resulted in minimal adjustments (Fig. 3c), outperforming the model using a Q_{10} equaling 1.8 that was shown to work best as an average setting across the entire domain. To better evaluate this variability and explore ways to reduce uncertainty in specific regions, we assessed the best parameterization fit with observations at the per grid-cell level (Fig. 4).

In our first analysis, we evaluated the spatial best fit model by keeping the baseline constant at a value of 0.35 and varying the CH_4 production Q_{10} values (Fig. 4a). This spatial analysis showed that, in general, in regions with large wetland areas and high annual CH_4 emissions (for example the Western Siberian Lowlands) a Q_{10} value of 1.4 resulted in the smallest model adjustment. As an increase in the Q_{10} parameter decreases CH_4 production for temperatures below 295 K, a higher Q_{10} value in these regions results in an underestimation of emissions. In contrast, regions such as Europe and northern Canada showed, in general, minimum model adjustments with a Q_{10} value of 2.2, suggesting that lower Q_{10} value would overestimate wetland CH_4 emissions in these regions. Interestingly, we observed adjustments with different signs in eastern Canada depending on the parameterization. For example, positive adjustments were associated with Q_{10} value of 2.2, as the prior emissions were underestimated compared with the estimated flux inferred from atmospheric observations. Additionally, we analyzed the effect of varying baseline flux values while keeping Q_{10} constant as 1.8, which showed that in high-emission areas, for example the Western Siberian Lowlands, in general a larger baseline flux value led to the smallest model adjustments (Fig. 4b). When considering the model adjustment for all sensitivity tests (varying both CH_4 production Q_{10} and baseline f_{CH_4} fraction) as shown in Fig. 4c, we also found a consistent pattern that confirmed the above findings varying only single parameters: the combination of higher baseline fluxes and lower Q_{10} value ($Q_{10} = 1.4$) best captured CH_4 dynamics in CH_4 hotspots, as the Western Siberia Lowlands.

The wide range of reported incubation-based Q_{10} values for CH_4 production in Arctic and northern wetlands depending on the site, substrate, and season, shows that the temperature sensitivity of CH_4 production varies considerably across environments (Bergman et al., 2000; Roy Chowdhury et al., 2015; Treat et al., 2015). This variability, which could be driven by factors such as vegetation type, organic matter quality, and microbial activity, emphasizes the necessity of models to account for spatial differences in process rates. For example, one synthesis study reported a mean Q_{10} value of 1.18 for CH_4 production under Arctic soil conditions (Treat et al., 2015). Roy Chowdhury et al. (2015) used anoxic laboratory incubations of active layer and permafrost samples from the Barrow Environmental Observatory in Alaska and reported a range of Q_{10} values from 1.8 to 22. Lupascu et al. (2012) reported that Q_{10} values describing the CH_4 production response of peat to a 10 °C temperature change ranged from 1.9 to 3.5 in sedge sites and from 2.4 to 5.8 in *Sphagnum* mire sites, and suggested that using spatially variable CH_4 production Q_{10} values could improve the accuracy of CH_4 flux modeling in northern wetlands. Furthermore, Bergman et al. (2000) found that the seasonal average Q_{10} values ranged from approximately 4.6 to 9.2 depending on the plant community of the various peat types. Here, our intent is not to directly compare our results with reported incubation-based values, since our adjustments in the CH_4 production Q_{10} refer to the Q_{10} of the CH_4:CO_2 production ratio, as represented in the model, and could not directly be comparable with CH_4 production Q_{10} from the literature review. In JSBACH, the Q_{10} applied to CH_4 production controls the fraction of CH_4 generated, but the surface emission ratio may still be lower due to oxidation and transport pathways. Together, these examples highlight that CH_4 production are strongly temperature dependent, and that the degree of this dependency can differ across regions and time periods. However, most current models cannot fully capture the influence of these factors due to structural limitations or a lack of detailed input data that is both spatially and temporally resolved. Consequently, these environmental drivers are often oversimplified or overlooked. Adjusting the CH_4 production Q_{10} values, as we do here, offers a useful initial approach, but it should not be seen as a long-term solution. Ideally, future model and data developments will enable CH_4 production Q_{10} values to adjust dynamically in response to underlying biophysical conditions, such as shifts in vegetation or organic matter characteristics. This will allow models to operate with a more generalizable formulation that still captures observed heterogeneity. Although our model experiments identified a single CH_4 production Q_{10} value that best agrees with observations at the pan-Arctic scale, they also showed that CH_4 emissions and model adjustments vary regionally. Some areas showed a substantial response to different Q_{10} values, which further demonstrates that an approach using a single parameter value is not sufficient.

https://doi.org/10.5194/egusphere-2025-4467
Preprint. Discussion started: 18 September 2025

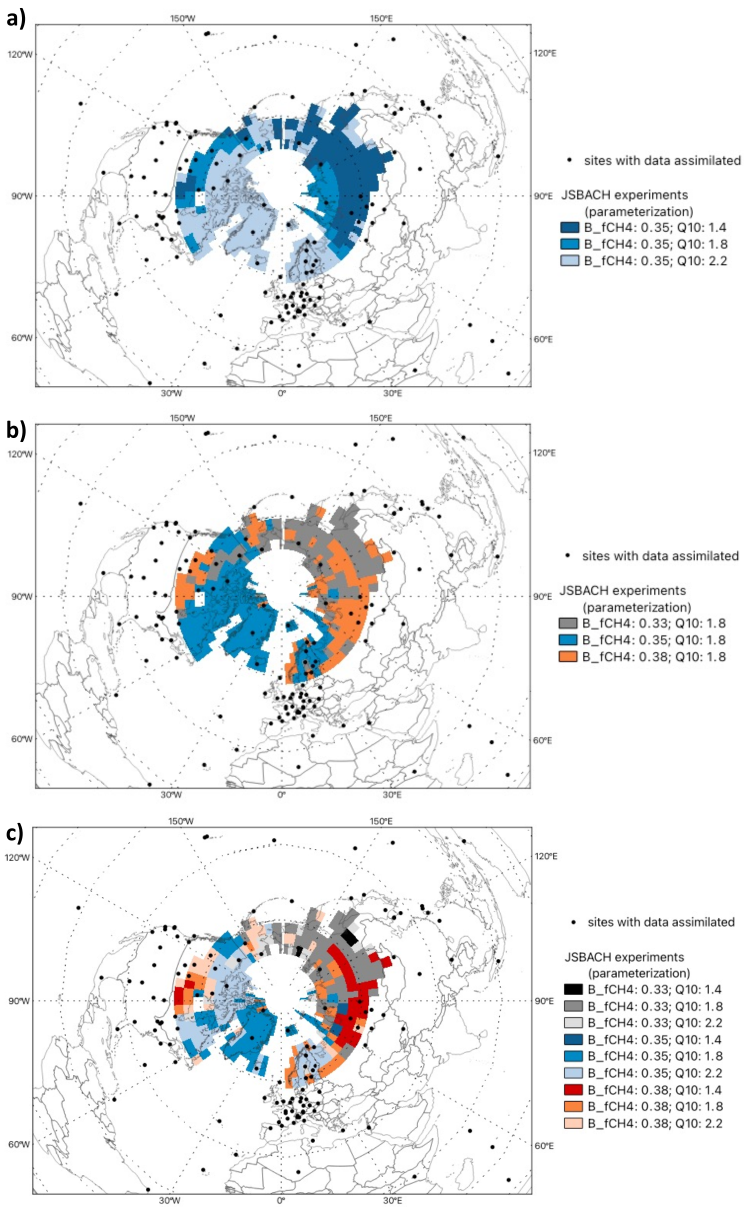

Figure 4. Map of the prior flux setting leading to minimum model adjustment (posterior minus prior fluxes) for the annual mean fluxes at each grid-cell for the Arctic-Boreal region varying the (a) CH_4 production Q_{10} parameter only, (b) baseline f_{CH_4} fraction only and (c) both Q_{10} parameter and baseline f_{CH_4} fraction.

https://doi.org/10.5194/egusphere-2025-4467
Preprint. Discussion started: 18 September 2025

4. Conclusions

Overall, our parameter sensitivity tests of bottom-up wetland emissions indicate that CH_4 production Q_{10} has a stronger effect on emission variability than the baseline f_{CH_4} fraction. Our bottom-up estimates showed that increasing CH_4 production Q_{10} from 1.4 to 2.2 decreased the annual mean wetland CH_4 emission in the Arctic–Boreal region by half. In addition, our analysis shows that a single Q_{10} value cannot capture the complexity of CH_4 emission dynamics across the Arctic-Boreal region. CH_4 production Q_{10} values of 1.8 and 2.2 underestimate hotspot emissions, mainly during summer. In contrast, a Q_{10} value of 1.4 overestimates emissions in regions with lower annual mean wetland emissions, such as e.g., Europe and northern Canada. Furthermore, a baseline f_{CH_4} fraction value of 0.38 led to the smallest model adjustments in CH_4 hotspots. These findings emphasize the importance of selecting appropriate parameterizations to accurately represent wetland emissions, especially in regions with substantial CH_4 release. Future models should incorporate dynamic, data-driven adjustments to reflect underlying environmental controls more accurately. If a varying CH_4 production Q_{10} value approach is not feasible for this region due to computational cost or model setup constraints, using a Q_{10} value of 1.8 provides the more similar CH_4 emission estimates compared to the atmospheric data across the entire Arctic-Boreal region.

Our analysis shows that atmospheric inverse modeling is a useful tool for evaluating and guiding process-model parameterizations when estimating wetland CH_4 emissions. However, it is important to note the limitations of the top-down approach. Top-down estimates rely heavily on the spatial and temporal distribution of atmospheric observations incorporated into the model. Regions with limited data or gaps, such as eastern Russia, can limit the ability to accurately identify emission sources and increase dependence on prior estimates. Global atmospheric inversions often operate at coarser spatial resolutions than the process models, and emission variability, including hotspot emissions, reducing the ability to estimate local scale process. At the grid-cell scale, assimilating only atmospheric CH_4 observations that is a result of total emissions (the balance between all sources and sinks) does not differentiate the overlapping source sectors in a grid-cell. However, differences in the spatial patterns and seasonality of emissions can be constrained by atmospheric CH_4 observations in inversions that solve for different sources categories (Saunois et al., 2025). Furthermore, errors in atmospheric transport model can propagate into emission estimates (Houweling et al., 1999; Locatelli et al., 2013; Schuh et al., 2019). Despite these limitations, our approach demonstrated a strong potential to help reduce the discrepancy between bottom-up and top-down estimates, therefore improving the accuracy of wetland CH_4 emission estimates.

5. Authors contributions

LSB, MG, GG, VB designed the methodology. LSB wrote the first version of the manuscript and performed analysis and CH_4 inversions. GG performed and provided the JSBACH simulations. CR provided guidance and technical support for the inverse modelling. CB provided additional input on the discussion of results. All authors contributed with analysis and text. MG supervised and acquired funding.

6. Competing interests

The authors declare that they have no conflict of interest.

7. Acknowledgements

The authors were funded by the European Research Council (ERC synergy project Q-Arctic, grant agreement no. 951288), the German Federal Ministry of Research, Technology and Space (MOMENT project, support code 03F0931G), and the AMPAC-net initiative (European Space Agency, grant no. 4000137912/22/I-DT). We would like to thank all Principal Investigators and supporting staff for setting up and maintaining observation sites around the world, particularly in the Arctic, and for making the data available through different databases. The authors would also like to thank Santiago Botía at MPI-BGC/BSI for his valuable comments and suggestions, which helped us to improve this manuscript. The authors would like to acknowledge the contributions of Tonatiuh Nunez Ramirez, who designed the CH_4 chemistry model for CarboScope inversion system used in this work. Parts of the text was language-edited for grammatical correctness using DeepL. The authors have reviewed and verified the content as needed and take full responsibility for it.

8. References

Bergman, I., Klarqvist, M., and Nilsson, M.: Seasonal variation in rates of methane production from peat of various botanical origins: effects of temperature and substrate quality, FEMS Microbiol Ecol, 33, 181–189, https://doi.org/10.1111/j.1574-6941.2000.tb00740.x, 2000.

Beven, K. J. and Kirkby, M. J.: A physically based, variable contributing area model of basin hydrology / Un modèle à base physique de zone d'appel variable de l'hydrologie du bassin versant, Hydrological Sciences Bulletin, 24, 43–69, https://doi.org/10.1080/02626667909491834, 1979.

Chinta, S., Gao, X., and Zhu, Q.: Machine Learning Driven Sensitivity Analysis of E3SM Land Model Parameters for Wetland Methane Emissions, J Adv Model Earth Syst, 16, https://doi.org/10.1029/2023MS004115, 2024.

Christensen, T. R., Prentice, I. C., Kaplan, J., Haxeltine, A., and Sitch, S.: Methane flux from northern wetlands and tundra, Tellus B: Chemical and Physical Meteorology, 48, 652, https://doi.org/10.3402/tellusb.v48i5.15938, 1996.

Conrad, R.: Contribution of hydrogen to methane production and control of hydrogen concentrations in methanogenic soils and sediments, FEMS Microbiol Ecol, 28, 193–202, https://doi.org/10.1111/j.1574-6941.1999.tb00575.x, 1999.

Conrad, R.: Importance of hydrogenotrophic, aceticlastic and methylotrophic methanogenesis for methane production in terrestrial, aquatic and other anoxic environments: A mini review, Pedosphere, 30, 25–39, https://doi.org/10.1016/S1002-0160(18)60052-9, 2020.

https://doi.org/10.5194/egusphere-2025-4467
Preprint. Discussion started: 18 September 2025

D'Imperio, L., Li, B.-B., Tiedje, J. M., Oh, Y., Christiansen, J. R., Kepfer-Rojas, S., Westergaard-Nielsen, A., Brandt, K. K., Holm, P. E., Wang, P., Ambus, P., and Elberling, B.: Spatial controls of methane uptake in upland soils across climatic and geological regions in Greenland, Commun Earth Environ, 4, 461, https://doi.org/10.1038/s43247-023-01143-3, 2023.

Ekici, A., Beer, C., Hagemann, S., Boike, J., Langer, M., and Hauck, C.: Simulating high-latitude permafrost regions by the JSBACH terrestrial ecosystem model, Geosci Model Dev, 7, 631–647, https://doi.org/10.5194/gmd-7-631-2014, 2014.

Etiope, G., Ciotoli, G., Schwietzke, S., and Schoell, M.: Gridded maps of geological methane emissions and their isotopic signature, Earth Syst Sci Data, 11, 1–22, https://doi.org/10.5194/essd-11-1-2019, 2019.

Goll, D. S., Brovkin, V., Liski, J., Raddatz, T., Thum, T., and Todd-Brown, K. E. O.: Strong dependence of CO_2 emissions from anthropogenic land cover change on initial land cover and soil carbon parametrization, Global Biogeochem Cycles, 29, 1511–1523, https://doi.org/10.1002/2014GB004988, 2015.

Gonzalez Moguel, R., Mahmoudi, N., and Douglas, P. M. J.: Large Variability in the Radiocarbon Signature of Greenhouse Gases From Incubations of Thermokarst Lake Sediments Linked to Methane Production Rates and CH_4:CO_2 Ratios, J Geophys Res Biogeosci, 130, https://doi.org/10.1029/2024JG008694, 2025.

Guimberteau, M., Zhu, D., Maignan, F., Huang, Y., Yue, C., Dantec-Nédélec, S., Ottlé, C., Jornet-Puig, A., Bastos, A., Laurent, P., Goll, D., Bowring, S., Chang, J., Guenet, B., Tifafi, M., Peng, S., Krinner, G., Ducharne, A., Wang, F., Wang, T., Wang, X., Wang, Y., Yin, Z., Lauerwald, R., Joetzjer, E., Qiu, C., Kim, H., and Ciais, P.: ORCHIDEE-MICT (v8.4.1), a land surface model for the high latitudes: model description and validation, Geosci Model Dev, 11, 121–163, https://doi.org/10.5194/gmd-11-121-2018, 2018.

Hagemann, S. and Stacke, T.: Impact of the soil hydrology scheme on simulated soil moisture memory, Clim Dyn, 44, 1731–1750, https://doi.org/10.1007/s00382-014-2221-6, 2015.

Harris, I. C.: CRUJRA: Collection of CRUJRA forcing datasets of gridded land surface blend of Climatic Research Unit (CRU) and Japanese reanalysis (JRA) data.Centre for Environmental Data Analysis, University of East Anglia Climatic Research Unit., 2019.

Heimann, M. and Körner, S.: The global atmospheric tracer model TM3: model description and user's manual release 3.8a, Jena, 2003.

Hossaini, R., Chipperfield, M. P., Saiz-Lopez, A., Fernandez, R., Monks, S., Feng, W., Brauer, P., and Glasow, R. von: A global model of tropospheric chlorine chemistry: Organic versus inorganic sources and impact on methane oxidation, Journal of Geophysical Research: Atmospheres, 121, 14,271-14,297, https://doi.org/10.1002/2016JD025756, 2016.

Houweling, S., Kaminski, T., Dentener, F., Lelieveld, J., and Heimann, M.: Inverse modeling of methane sources and sinks using the adjoint of a global transport model, Journal of Geophysical Research: Atmospheres, 104, 26137–26160, https://doi.org/10.1029/1999JD900428, 1999.

Houweling, S., Bergamaschi, P., Chevallier, F., Heimann, M., Kaminski, T., Krol, M., Michalak, A. M., and Patra, P.: Global inverse modeling of CH_4 sources and sinks: an overview of methods, Atmos Chem Phys, 17, 235–256, https://doi.org/10.5194/acp-17-235-2017, 2017.

https://doi.org/10.5194/egusphere-2025-4467
Preprint. Discussion started: 18 September 2025

Hugelius, G., Ramage, J., Burke, E., Chatterjee, A., Smallman, T. L., Aalto, T., Bastos, A., Biasi, C., Canadell, J. G., Chandra, N., Chevallier, F., Ciais, P., Chang, J., Feng, L., Jones, M. W., Kleinen, T., Kuhn, M., Lauerwald, R., Liu, J., López-Blanco, E., Luijkx, I. T., Marushchak, M. E., Natali, S. M., Niwa, Y., Olefeldt, D., Palmer, P. I., Patra, P. K., Peters, W., Potter, S., Poulter, B., Rogers, B. M., Riley, W. J., Saunois, M., Schuur, E. A. G., Thompson, R. L., Treat, C., Tsuruta, A., Turetsky, M. R., Virkkala, A. -M., Voigt, C., Watts, J., Zhu, Q., and Zheng, B.: Permafrost Region Greenhouse Gas Budgets Suggest a Weak CO_2 Sink and CH_4 and N_2O Sources, But Magnitudes Differ Between Top-Down and Bottom-Up Methods, Global Biogeochem Cycles, 38, https://doi.org/10.1029/2023GB007969, 2024.

ICOS RI, Bergamaschi, P., Colomb, A., De Mazière, M., Emmenegger, L., Kubistin, D., Lehner, I., Lehtinen, K., Lund Myhre, C., Marek, M., O'Doherty, S., Platt, S. M., Plaß-Dülmer, C., Ramonet, M., Apadula, F., Arnold, S., Blanc, P.-E., Brunner, D., Chen, H., …, and ICOS Central Radiocarbon Laboratory.: European Obspack compilation of atmospheric methane data from ICOS and non-ICOS European stations for the period 1984-2024; obspack_ch4_466_GVeu_2024-02-01 (Version 1.0) [Data set]. ICOS ERIC - Carbon Portal, 2024.

IEA, Crippa, M., Guizzardi, D., Pagani, F., Banja, M., and et al.: GHG emissions of all world countries, Publications Office of the European Union, https://doi.org/https://data.europa.eu/doi/10.2760/4002897, 2024.

Jöckel, P., Tost, H., Pozzer, A., Brühl, C., Buchholz, J., Ganzeveld, L., Hoor, P., Kerkweg, A., Lawrence, M. G., Sander, R., Steil, B., Stiller, G., Tanarhte, M., Taraborrelli, D., van Aardenne, J., and Lelieveld, J.: The atmospheric chemistry general circulation model ECHAM5/MESSy1: consistent simulation of ozone from the surface to the mesosphere, Atmos Chem Phys, 6, 5067–5104, https://doi.org/10.5194/acp-6-5067-2006, 2006.

Juncher Jørgensen, C., Schlaikjær Mariager, T., and Riis Christiansen, J.: Spatial variation of net methane uptake in Arctic and subarctic drylands of Canada and Greenland, Geoderma, 443, 116815, https://doi.org/10.1016/j.geoderma.2024.116815, 2024.

Kaiser, S., Göckede, M., Castro-Morales, K., Knoblauch, C., Ekici, A., Kleinen, T., Zubrzycki, S., Sachs, T., Wille, C., and Beer, C.: Process-based modelling of the methane balance in periglacial landscapes (JSBACH-methane), Geosci Model Dev, 10, 333–358, https://doi.org/10.5194/gmd-10-333-2017, 2017.

Kalnay, E., Kanamitsu, M., Kistler, R., Collins, W., Deaven, D., Gandin, L., Iredell, M., Saha, S., White, G., Woollen, J., Zhu, Y., Leetmaa, A., Reynolds, R., Chelliah, M., Ebisuzaki, W., Higgins, W., Janowiak, J., Mo, K. C., Ropelewski, C., Wang, J., Jenne, R., and Joseph, D.: The NCEP/NCAR 40-Year Reanalysis Project, Bull Am Meteorol Soc, 77, 437–471, https://doi.org/10.1175/1520-0477(1996)077<0437:TNYRP>2.0.CO;2, 1996.

Kim, H.-S., Maksyutov, S., Glagolev, M. V, Machida, T., Patra, P. K., Sudo, K., and Inoue, G.: Evaluation of methane emissions from West Siberian wetlands based on inverse modeling, Environmental Research Letters, 6, 035201, https://doi.org/10.1088/1748-9326/6/3/035201, 2011.

Kleinen, T., Mikolajewicz, U., and Brovkin, V.: Terrestrial methane emissions from the Last Glacial Maximum to the preindustrial period, Climate of the Past, 16, 575–595, https://doi.org/10.5194/cp-16-575-2020, 2020.

https://doi.org/10.5194/egusphere-2025-4467
Preprint. Discussion started: 18 September 2025

Knoblauch, C., Spott, O., Evgrafova, S., Kutzbach, L., and Pfeiffer, E.: Regulation of methane production, oxidation, and emission by vascular plants and bryophytes in ponds of the northeast Siberian polygonal tundra, J Geophys Res Biogeosci, 120, 2525–2541, https://doi.org/10.1002/2015JG003053, 2015.

Knoblauch, C., Beer, C., Liebner, S., Grigoriev, M. N., and Pfeiffer, E.-M.: Methane production as key to the greenhouse gas budget of thawing permafrost, Nat Clim Chang, 8, 309–312, https://doi.org/10.1038/s41558-018-0095-z, 2018.

Locatelli, R., Bousquet, P., Chevallier, F., Fortems-Cheney, A., Szopa, S., Saunois, M., Agusti-Panareda, A., Bergmann, D., Bian, H., Cameron-Smith, P., Chipperfield, M. P., Gloor, E., Houweling, S., Kawa, S. R., Krol, M., Patra, P. K., Prinn, R. G., Rigby, M., Saito, R., and Wilson, C.: Impact of transport model errors on the global and regional methane emissions estimated by inverse modelling, Atmos Chem Phys, 13, 9917–9937, https://doi.org/10.5194/acp-13-9917-2013, 2013.

Lupascu, M., Wadham, J. L., Hornibrook, E. R. C., and Pancost, R. D.: Temperature Sensitivity of Methane Production in the Permafrost Active Layer at Stordalen, Sweden: A Comparison with Non-permafrost Northern Wetlands, Arct Antarct Alp Res, 44, 469–482, https://doi.org/10.1657/1938-4246-44.4.469, 2012.

Mauritsen, T., Bader, J., Becker, T., Behrens, J., Bittner, M., Brokopf, R., Brovkin, V., Claussen, M., Crueger, T., Esch, M., Fast, I., Fiedler, S., Fläschner, D., Gayler, V., Giorgetta, M., Goll, D. S., Haak, H., Hagemann, S., Hedemann, C., Hohenegger, C., Ilyina, T., Jahns, T., Jimenéz-de-la-Cuesta, D., Jungclaus, J., Kleinen, T., Kloster, S., Kracher, D., Kinne, S., Kleberg, D., Lasslop, G., Kornblueh, L., Marotzke, J., Matei, D., Meraner, K., Mikolajewicz, U., Modali, K., Möbis, B., Müller, W. A., Nabel, J. E. M. S., Nam, C. C. W., Notz, D., Nyawira, S., Paulsen, H., Peters, K., Pincus, R., Pohlmann, H., Pongratz, J., Popp, M., Raddatz, T. J., Rast, S., Redler, R., Reick, C. H., Rohrschneider, T., Schemann, V., Schmidt, H., Schnur, R., Schulzweida, U., Six, K. D., Stein, L., Stemmler, I., Stevens, B., von Storch, J., Tian, F., Voigt, A., Vrese, P., Wieners, K., Wilkenskjeld, S., Winkler, A., and Roeckner, E.: Developments in the MPI-M Earth System Model version 1.2 (MPI-ESM1.2) and Its Response to Increasing CO_2, J Adv Model Earth Syst, 11, 998–1038, https://doi.org/10.1029/2018MS001400, 2019.

Miller, S. M., Commane, R., Melton, J. R., Andrews, A. E., Benmergui, J., Dlugokencky, E. J., Janssens-Maenhout, G., Michalak, A. M., Sweeney, C., and Worthy, D. E. J.: Evaluation of wetland methane emissions across North America using atmospheric data and inverse modeling, Biogeosciences, 13, 1329–1339, https://doi.org/10.5194/bg-13-1329-2016, 2016.

Moser, M., Kaiser, L., Brovkin, V., and Beer, C.: Reviews and syntheses: Process-based modeling of the CO_2:CH_4 production ratio is important for predicting future Arctic methane emissions, https://doi.org/10.5194/egusphere-2025-3159, 2025.

Olefeldt, D., Hovemyr, M., Kuhn, M. A., Bastviken, D., Bohn, T. J., Connolly, J., Crill, P., Euskirchen, E. S., Finkelstein, S. A., Genet, H., Grosse, G., Harris, L. I., Heffernan, L., Helbig, M., Hugelius, G., Hutchins, R., Juutinen, S., Lara, M. J., Malhotra, A., Manies, K., McGuire, A. D., Natali, S. M., O'Donnell, J. A., Parmentier, F.-J. W., Räsänen, A., Schädel, C., Sonnentag, O., Strack, M., Tank, S. E., Treat, C., Varner, R. K., Virtanen, T., Warren, R. K., and Watts, J. D.: The Boreal–Arctic Wetland and Lake Dataset (BAWLD), Earth Syst Sci Data, 13, 5127–5149, https://doi.org/10.5194/essd-13-5127-2021, 2021.

Poulter, B., Bousquet, P., Canadell, J. G., Ciais, P., Peregon, A., Saunois, M., Arora, V. K., Beerling, D. J., Brovkin, V., Jones, C. D., Joos, F., Gedney, N., Ito, A., Kleinen, T., Koven, C. D., McDonald, K., Melton, J. R., Peng, C., Peng, S., Prigent, C.,

https://doi.org/10.5194/egusphere-2025-4467
Preprint. Discussion started: 18 September 2025

Schroeder, R., Riley, W. J., Saito, M., Spahni, R., Tian, H., Taylor, L., Viovy, N., Wilton, D., Wiltshire, A., Xu, X., Zhang, B., Zhang, Z., and Zhu, Q.: Global wetland contribution to 2000–2012 atmospheric methane growth rate dynamics, Environmental Research Letters, 12, 094013, https://doi.org/10.1088/1748-9326/aa8391, 2017.

Reick, C. H., Gayler, V., Goll, D., Hagemann, S., Heidkamp, M., Nabel, J. E. M. S., Raddatz, T., Roeckner, E., Schnur, R., and Wilkenskjeld, S.: JSBACH 3 - The land component of the MPI Earth System Model: documentation of version 3.2, 2021.

Ricciuto, D. M., Xu, X., Shi, X., Wang, Y., Song, X., Schadt, C. W., Griffiths, N. A., Mao, J., Warren, J. M., Thornton, P. E., Chanton, J., Keller, J. K., Bridgham, S. D., Gutknecht, J., Sebestyen, S. D., Finzi, A., Kolka, R., and Hanson, P. J.: An Integrative Model for Soil Biogeochemistry and Methane Processes: I. Model Structure and Sensitivity Analysis, J Geophys Res Biogeosci, 126, https://doi.org/10.1029/2019JG005468, 2021.

Richards, L. A.: CAPILLARY CONDUCTION OF LIQUIDS THROUGH POROUS MEDIUMS, Physics (College Park Md), 1, 318–333, https://doi.org/10.1063/1.1745010, 1931.

Riley, W. J., Subin, Z. M., Lawrence, D. M., Swenson, S. C., Torn, M. S., Meng, L., Mahowald, N. M., and Hess, P.: Barriers to predicting changes in global terrestrial methane fluxes: analyses using CLM4Me, a methane biogeochemistry model integrated in CESM, Biogeosciences, 8, 1925–1953, https://doi.org/10.5194/bg-8-1925-2011, 2011.

Rödenbeck, C.: Estimating CO2 sources and sinks from atmospheric mixing ratio measurements using a global inversion of atmospheric transport, Jena, 2005.

Roy Chowdhury, T., Herndon, E. M., Phelps, T. J., Elias, D. A., Gu, B., Liang, L., Wullschleger, S. D., and Graham, D. E.: Stoichiometry and temperature sensitivity of methanogenesis and <scp>CO</scp> $_2$ production from saturated polygonal tundra in Barrow, Alaska, Glob Chang Biol, 21, 722–737, https://doi.org/10.1111/gcb.12762, 2015.

Saunois, M., Martinez, A., Poulter, B., Zhang, Z., Raymond, P. A., Regnier, P., Canadell, J. G., Jackson, R. B., Patra, P. K., Bousquet, P., Ciais, P., Dlugokencky, E. J., Lan, X., Allen, G. H., Bastviken, D., Beerling, D. J., Belikov, D. A., Blake, D. R., Castaldi, S., Crippa, M., Deemer, B. R., Dennison, F., Etiope, G., Gedney, N., Höglund-Isaksson, L., Holgerson, M. A., Hopcroft, P. O., Hugelius, G., Ito, A., Jain, A. K., Janardanan, R., Johnson, M. S., Kleinen, T., Krummel, P. B., Lauerwald, R., Li, T., Liu, X., McDonald, K. C., Melton, J. R., Mühle, J., Müller, J., Murguia-Flores, F., Niwa, Y., Noce, S., Pan, S., Parker, R. J., Peng, C., Ramonet, M., Riley, W. J., Rocher-Ros, G., Rosentreter, J. A., Sasakawa, M., Segers, A., Smith, S. J., Stanley, E. H., Thanwerdas, J., Tian, H., Tsuruta, A., Tubiello, F. N., Weber, T. S., van der Werf, G. R., Worthy, D. E. J., Xi, Y., Yoshida, Y., Zhang, W., Zheng, B., Zhu, Q., Zhu, Q., and Zhuang, Q.: Global Methane Budget 2000–2020, Earth Syst Sci Data, 17, 1873–1958, https://doi.org/10.5194/essd-17-1873-2025, 2025.

Schuh, A. E., Jacobson, A. R., Basu, S., Weir, B., Baker, D., Bowman, K., Chevallier, F., Crowell, S., Davis, K. J., Deng, F., Denning, S., Feng, L., Jones, D., Liu, J., and Palmer, P. I.: Quantifying the Impact of Atmospheric Transport Uncertainty on CO_2 Surface Flux Estimates, Global Biogeochem Cycles, 33, 484–500, https://doi.org/10.1029/2018GB006086, 2019.

Schuldt, K. N., Mund, J., Aalto, T., Andrews, A., Apadula, F., Jgor Arduini, Arnold, S., Baier, B., Bäni, L., Bartyzel, J., Bergamaschi, P., Biermann, T., Biraud, S. C., Pierre-Eric Blanc, Boenisch, H., Brailsford, G., Brand, W. A., Brunner, D., Bui,

https://doi.org/10.5194/egusphere-2025-4467
Preprint. Discussion started: 18 September 2025

T. P. V., and Miroslaw Zimnoch: Multi-laboratory compilation of atmospheric carbon dioxide data for the period 1983-2022; obspack_ch4_1_GLOBALVIEWplus_v6.0_2023-12-01 [Data set]. NOAA Global Monitoring Laboratory., 2023.

Sellar, A. A., Jones, C. G., Mulcahy, J. P., Tang, Y., Yool, A., Wiltshire, A., O'Connor, F. M., Stringer, M., Hill, R., Palmieri, J., Woodward, S., de Mora, L., Kuhlbrodt, T., Rumbold, S. T., Kelley, D. I., Ellis, R., Johnson, C. E., Walton, J., Abraham, N. L., Andrews, M. B., Andrews, T., Archibald, A. T., Berthou, S., Burke, E., Blockley, E., Carslaw, K., Dalvi, M., Edwards, J., Folberth, G. A., Gedney, N., Griffiths, P. T., Harper, A. B., Hendry, M. A., Hewitt, A. J., Johnson, B., Jones, A., Jones, C. D., Keeble, J., Liddicoat, S., Morgenstern, O., Parker, R. J., Predoi, V., Robertson, E., Siahaan, A., Smith, R. S., Swaminathan, R., Woodhouse, M. T., Zeng, G., and Zerroukat, M.: UKESM1: Description and Evaluation of the U.K. Earth System Model, J Adv Model Earth Syst, 11, 4513–4558, https://doi.org/10.1029/2019MS001739, 2019.

Song, C., Luan, J., Xu, X., Ma, M., Aurela, M., Lohila, A., Mammarella, I., Alekseychik, P., Tuittila, E., Gong, W., Chen, X., Meng, X., and Yuan, W.: A Microbial Functional Group-Based CH_4 Model Integrated Into a Terrestrial Ecosystem Model: Model Structure, Site-Level Evaluation, and Sensitivity Analysis, J Adv Model Earth Syst, 12, https://doi.org/10.1029/2019MS001867, 2020.

Song, H., Peng, C., Zhu, Q., Chen, Z., Blanchet, J.-P., Liu, Q., Li, T., Li, P., and Liu, Z.: Quantification and uncertainty of global upland soil methane sinks: Processes, controls, model limitations, and improvements, Earth Sci Rev, 252, 104758, https://doi.org/10.1016/j.earscirev.2024.104758, 2024.

Spahni, R., Wania, R., Neef, L., van Weele, M., Pison, I., Bousquet, P., Frankenberg, C., Foster, P. N., Joos, F., Prentice, I. C., and van Velthoven, P.: Constraining global methane emissions and uptake by ecosystems, Biogeosciences, 8, 1643–1665, https://doi.org/10.5194/bg-8-1643-2011, 2011.

Spivakovsky, C. M., Logan, J. A., Montzka, S. A., Balkanski, Y. J., Foreman-Fowler, M., Jones, D. B. A., Horowitz, L. W., Fusco, A. C., Brenninkmeijer, C. A. M., Prather, M. J., Wofsy, S. C., and McElroy, M. B.: Three-dimensional climatological distribution of tropospheric OH: Update and evaluation, Journal of Geophysical Research: Atmospheres, 105, 8931–8980, https://doi.org/10.1029/1999JD901006, 2000.

Sulman, B. N., Yuan, F., O'Meara, T., Gu, B., Herndon, E. M., Zheng, J., Thornton, P. E., and Graham, D. E.: Simulated Hydrological Dynamics and Coupled Iron Redox Cycling Impact Methane Production in an Arctic Soil, J Geophys Res Biogeosci, 127, https://doi.org/10.1029/2021JG006662, 2022.

Treat, C. C., Natali, S. M., Ernakovich, J., Iversen, C. M., Lupascu, M., McGuire, A. D., Norby, R. J., Roy Chowdhury, T., Richter, A., Šantrůčková, H., Schädel, C., Schuur, E. A. G., Sloan, V. L., Turetsky, M. R., and Waldrop, M. P.: A pan-Arctic synthesis of CH_4 and CO_2 production from anoxic soil incubations, Glob Chang Biol, 21, 2787–2803, https://doi.org/10.1111/gcb.12875, 2015.

Tuomi, M., Rasinmäki, J., Repo, A., Vanhala, P., and Liski, J.: Soil carbon model Yasso07 graphical user interface, Environmental Modelling & Software, 26, 1358–1362, https://doi.org/10.1016/j.envsoft.2011.05.009, 2011.

Vogt, J., Pallandt, M. M. T. A., Basso, L. S., Bolek, A., Ivanova, K., Schlutow, M., Celis, G., Kuhn, M., Mauritz, M., Schuur, E. A. G., Arndt, K., Virkkala, A.-M., Wargowsky, I., and Göckede, M.: ARGO: ARctic greenhouse Gas Observation metadata version 1, Earth Syst Sci Data, 17, 2553–2573, https://doi.org/10.5194/essd-17-2553-2025, 2025.

Voigt, C., Virkkala, A.-M., Hould Gosselin, G., Bennett, K. A., Black, T. A., Detto, M., Chevrier-Dion, C., Guggenberger, G., Hashmi, W., Kohl, L., Kou, D., Marquis, C., Marsh, P., Marushchak, M. E., Nesic, Z., Nykänen, H., Saarela, T., Sauheitl, L., Walker, B., Weiss, N., Wilcox, E. J., and Sonnentag, O.: Arctic soil methane sink increases with drier conditions and higher ecosystem respiration, Nat Clim Chang, 13, 1095–1104, https://doi.org/10.1038/s41558-023-01785-3, 2023.

Walter, B. P. and Heimann, M.: A process-based, climate-sensitive model to derive methane emissions from natural wetlands: Application to five wetland sites, sensitivity to model parameters, and climate, Global Biogeochem Cycles, 14, 745–765, https://doi.org/10.1029/1999GB001204, 2000.

Wania, R., Ross, I., and Prentice, I. C.: Implementation and evaluation of a new methane model within a dynamic global vegetation model: LPJ-WHyMe v1.3.1, Geosci Model Dev, 3, 565–584, https://doi.org/10.5194/gmd-3-565-2010, 2010.

Weber, T., Wiseman, N. A., and Kock, A.: Global ocean methane emissions dominated by shallow coastal waters, Nat Commun, 10, 4584, https://doi.org/10.1038/s41467-019-12541-7, 2019.

Ying, Q., Poulter, B., Watts, J. D., Arndt, K. A., Virkkala, A.-M., Bruhwiler, L., Oh, Y., Rogers, B. M., Natali, S. M., Sullivan, H., Armstrong, A., Ward, E. J., Schiferl, L. D., Elder, C. D., Peltola, O., Bartsch, A., Desai, A. R., Euskirchen, E., Göckede, M., Lehner, B., Nilsson, M. B., Peichl, M., Sonnentag, O., Tuittila, E.-S., Sachs, T., Kalhori, A., Ueyama, M., and Zhang, Z.: WetCH$_4$: a machine-learning-based upscaling of methane fluxes of northern wetlands during 2016–2022, Earth Syst Sci Data, 17, 2507–2534, https://doi.org/10.5194/essd-17-2507-2025, 2025.

Yuan, K., Li, F., McNicol, G., Chen, M., Hoyt, A., Knox, S., Riley, W. J., Jackson, R., and Zhu, Q.: Boreal–Arctic wetland methane emissions modulated by warming and vegetation activity, Nat Clim Chang, 14, 282–288, https://doi.org/10.1038/s41558-024-01933-3, 2024.

Zhang, Z., Poulter, B., Melton, J. R., Riley, W. J., Allen, G. H., Beerling, D. J., Bousquet, P., Canadell, J. G., Fluet-Chouinard, E., Ciais, P., Gedney, N., Hopcroft, P. O., Ito, A., Jackson, R. B., Jain, A. K., Jensen, K., Joos, F., Kleinen, T., Knox, S. H., Li, T., Li, X., Liu, X., McDonald, K., McNicol, G., Miller, P. A., Müller, J., Patra, P. K., Peng, C., Peng, S., Qin, Z., Riggs, R. M., Saunois, M., Sun, Q., Tian, H., Xu, X., Yao, Y., Xi, Y., Zhang, W., Zhu, Q., Zhu, Q., and Zhuang, Q.: Ensemble estimates of global wetland methane emissions over 2000–2020, Biogeosciences, 22, 305–321, https://doi.org/10.5194/bg-22-305-2025, 2025.

Zheng, J., Thornton, P. E., Painter, S. L., Gu, B., Wullschleger, S. D., and Graham, D. E.: Modeling anaerobic soil organic carbon decomposition in Arctic polygon tundra: insights into soil geochemical influences on carbon mineralization, Biogeosciences, 16, 663–680, https://doi.org/10.5194/bg-16-663-2019, 2019.